Fatigue crack initiation and early growth in a multiphase Al alloy included in a multilayer material system

M. R. Joyce, S. Syngellakis and P. A. S. Reed

The fatigue properties of a multilayer material system employed in the manufacture of small automotive plain bearings are assessed. This comprised three layers; a multiphase Al–Sn–Si lining, a bonding Al interlayer, and a steel backing. The structure was found to exhibit complex fatigue behaviour; including multiple crack initiations, highly microstructural crack growth, and complex crack interaction, coalescence, and deflection events. Key microstructural features are identified for both initiation and early propagation of fatigue cracks within the lining material. The effects of both the layered structure and service environment on fatigue crack propagation behaviour are assessed. This provides valuable information for the development of new lining alloys for future automotive bearing designs.

MST/5468

Keywords: Fatigue crack initiation, Fatigue crack growth, Al–Sn–Si alloys

Dr Joyce and Dr Reed are in the Materials Research Group and Dr Syngellakis is in the Computational Engineering and Design Group, School of Engineering Sciences, University of Southampton, Highfield, Southampton, SO17 1BJ, UK (mrj1@soton.ac.uk). *Manuscript received 19 March 2002; accepted 27 August 2003.*

Introduction

Due to advances in material selection, plain bearing fatigue failures in small automotive engines are not currently observed in service. However, car manufacturers are constantly striving to both increase the power output and reduce the weight of next generation engines. It is recognised that these measures will require increases in the service loading for crankshaft and big-end plain bearings, leading to the possibility of fatigue failure in current bearing designs.[1] Layered material systems are used extensively as crankcase main bearings in small automotive engines. The system considered in this paper is typical of a modern bearing design in that it employs three layers; an Al–Sn–Si lining material, a nominally pure Al interlayer, and a steel backing layer, as shown schematically in Fig. 1.

It is thought that bearing fatigue failure may be caused by cyclic stresses in the bearing lining arising from the unstable nature of the hydrodynamic oil film.[2] Typically fatigue cracks will initiate therefore at multiple points on the bearing surface, and the coalescence and subsurface growth of these cracks may cause sections of lining to detach (spall), precipitating bearing failure.[1]

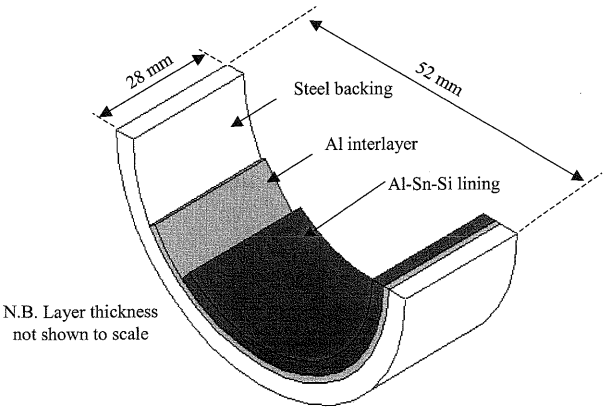

1 Schematic of shell bearing construction

Bearing fatigue performance is generally assessed using artificial accelerated test rigs, which aim to simulate service loading, but allow its magnitude to be increased to a level causing rapid bearing failure. Generally, the bearing under test is mounted on a rotating eccentric shaft and loaded via a hydraulic actuator. This allows a combination of rotating and reciprocating load to be applied. However, the enclosed nature of such machines precludes the detailed monitoring required to characterise fatigue behaviour. Indeed failure is usually detected by an increase in lubricating oil temperature, indicating that the bearing is beginning to seize. Bearing material systems have been developed over many years using such a total component life approach, however as their construction becomes more complex comprising several layers and multiphase materials, this semiempirical approach becomes harder to implement successfully. In the work presented here, no attempt was made to simulate service loading; rather the fundamental fatigue behaviour of a typical bearing material system was assessed under simple and well characterised loading conditions.

Material characterisation

Dana Glacier Vandervell produce the bearings considered in this work by a proprietary route, and therefore complete processing details cannot be made available. However the route employed is typical for this type of system.[3] The Al–Sn–Si lining is continuously cast, cut into billets, and homogenised. The lining material is then extensively cold worked to reduce its thickness, break up weak grain boundary Sn films and to disrupt the tenacious surface oxide, which would otherwise prevent secure bonding to the steel backing layer. Due to the severity of the rolling process Sn smearing occurs, therefore nominally pure Al layers are incorporated on the upper and lower surfaces during the rolling process. One of these forms the interlayer to ensure good bonding with the steel backing, while the other is machined away in the bearing finishing operation. The lining is roll bonded to the steel backing, after which it undergoes a final annealing treatment to recrystallise the

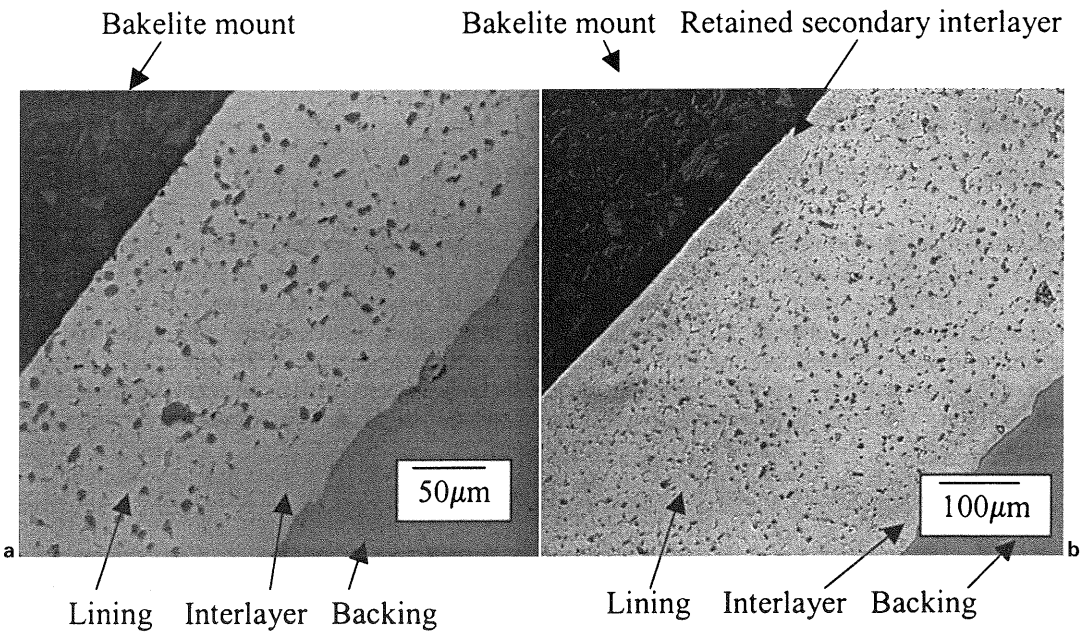

a bearing; *b* flat strip

2 Sections through as received materials showing layered structure

lining alloy. The layered material is then formed into bearings and broached to give the desired lining thickness. The finished bearings used in this study have an outer diameter of 52 mm and a breadth of 28 mm. In addition to finished bearings, the layered material was also available for testing as a flat sheet (in the condition immediately prior to the bearing forming operation). Figure 2*a* and 2*b* show sections through the as received bearings and flat strip materials respectively. In both cases individual material layers are easily distinguished, although the interfaces between them are not completely smooth. The interlayer is the secondary phase free region adjacent to the steel backing as indicated. Comparing the two structures, it may be seen that the lining of the flat strip materials is considerably thicker and retains the second pure Al layer, while this has been machined away in the finished bearings. The respective layer thicknesses of bearings and flat strip material are given in Table 1.

Figure 3 shows an optical micrograph of a polished and unetched section of bearing lining material. It is clear that this material is multiphase, with Si and the Sn existing as two distinct secondary phases. The silicon phase is spheroidal and apparently uniformly distributed. Image analysis showed that the mean Si size was 7·75 μm^2 with a standard deviation of 6·06 μm^2. The lighter grey reticular phase is Sn. This is often seen to be associated with the Si phases, occasionally encapsulating them entirely.

A polished and unetched section of bearing lining microstructure was examined using a Jeol 6400 SEM at an accelerating voltage of 20 kV; Fig. 4 shows a backscattered image (BEI) of the sample surface. The secondary phases may clearly be distinguished by this method, and to confirm their composition, energy dispersive X-ray (EDX) spectra were obtained from the four points indicated. The spectra

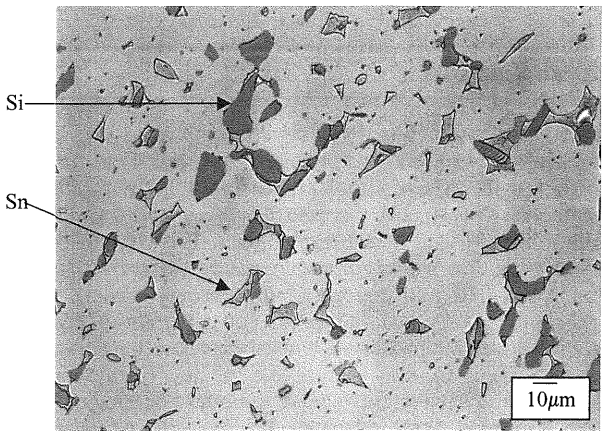

3 Optical micrograph of bearing lining microstructure

from point 1 revealed that the matrix comprised Al as expected, together with small amounts of Fe and Cu. The spectra from points 2 and 3 showed that these phases were exclusively Si and Sn, respectively, as expected. Finally, the spectra from point 4 identified this particle as an intermetallic containing predominantly Al, with lesser and approximately equal quantities of Si and Fe. Based on this and with reference to a phase diagram it is likely that this is $FeSiAl_5$.

The material properties of the Al alloy lining material and the steel backing were determined by tensile testing; this involved grinding away the unwanted layers of material to leave either the backing or lining as a monolithic sheet. Due to the thinness of the interlayer it was not possible to determine its properties in this manner. In discussion with

Table 1 Measured material properties and layer thicknesses in as supplied bearings and flat strip

	Layer thickness, mm					
Material	Bearing	Flat strip	Young's modulus, Gpa	Poisson's ratio	Yield stress, MPa	Ultimate tensile stress, MPa
Al–Sn–Si lining	0·244	0·46	69·8	0·33	56·6	187·5
Al interlayer	0·06	0·06	70·0	0·30	33·8	77·8
Steel backing	1·51	1·51	207·0	0·30	350·0	520·0

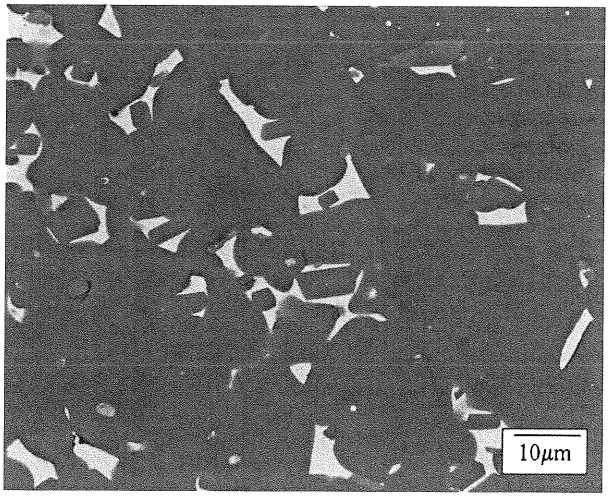

4 Backscattered SEM image of bearing lining microstructure

the sponsoring company and after examining the results of microhardness indents, it was assumed that this layer had similar mechanical properties to pure Al in the O temper. The material properties for each layer are given in Table 1.

Fatigue testing

A detailed programme of testing was carried out to characterise the fundamental fatigue behaviour of the bearing material system, including uninterrupted to failure fatigue tests on finished bearings; interrupted short crack fatigue tests in air, performed in bend on flat strip samples; and interrupted short crack fatigue bend tests, performed on flat strip samples in *vacuo* and in an oil environment.

The runout tests on as received bearings were used to generate S – N type data, however, due to difficulties achieving a high quality polish on the curved lining surface, the bearings were unsuitable for crack monitoring via acetate replication. Hence flat strip samples were used for the interrupted test programme in air, vacuum, and oil environments.

BEARING TESTS

These tests were carried out in a three point bend loading geometry, using a steel block to constrain the ends of the bearing, as shown in Fig. 5*a*. Since a large number of tests were anticipated, the use of a rig ensured an identical test set up for each sample. The tests were carried out using a 50 kN Instron 8501, at 10 Hz with a load ratio of 0·1.

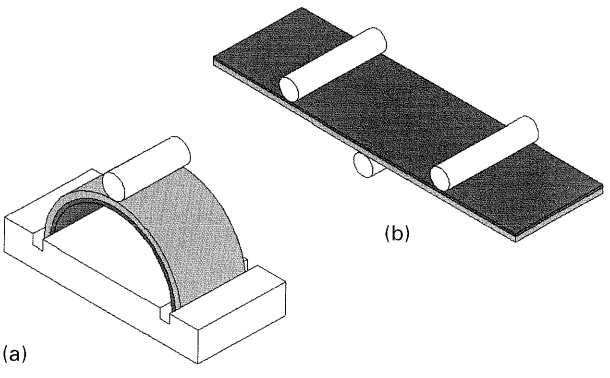

a bearing test rig; *b* three point bend rig

5 Simplified loading geometries

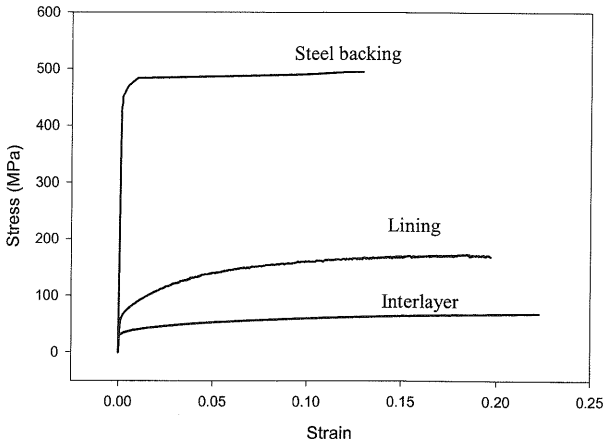

6 Material response curves for FE modelling

In the test geometry adopted for the bearing tests, the region of maximum tensile lining stress is at the free surface directly below the upper roller. Calculating the magnitude of this stress is, however, non-trivial. Therefore it was evaluated using a simple elastoplastic finite element model. This model was created using the ANSYS5.7 general purpose finite element (FE) code, and considered a 2D section through the bearing. The three material layers were modelled discretely; their widths are given in Table 1. Approximately 800 eight noded quadrilateral elements formulated for plane strain were used to mesh the model. Cyclic material properties were not available, rather, isotropic plasticity was employed using monotonic multilinear curves for each material layer, which are shown in Fig. 6. The free end of the bearing where it is supported by the block was constrained in both axes, while a static point load was applied at the apex. This load was monotonically increased from 0 to maximum without unloading, and the tensile stress at the lining surface evaluated. The results are plotted in Fig. 7.

To obtain $S-N$ type data a series of runout tests were carried out under constant load range conditions, at predicted maximum lining stresses between 80 and 155 MPa. To ensure that all these tests were terminated at a similar amount of fatigue damage, a failure criterion was required. Due to both the lining surface roughness and the large number of tests, acetate replication was not suitable for crack monitoring, and thus a compliance method was employed. The sample displacement at maximum load was recorded throughout the test. When this value had increased by 0·3 mm, the sample was deemed to have failed. Generally at this point, the lining was found to have visible cracks across its width and a dominant crack had entered the steel backing. However, gross sample deformation had not taken place, and hence the fatigue crack morphology was preserved for post-test examination.

FLAT STRIP SHORT CRACK TESTS

Bend bar type specimens of dimensions 80 mm by 20 mm were produced from the flat strip material. The surface of the lining material was then ground back and polished to remove the retained secondary interlayer and to reduce the lining thickness to that of a finished bearing (~0·25 mm). Tests were performed using a three point bend loading geometry, shown in Fig. 5*b*, with a loading span of 25 mm. In common with the earlier bearing tests, an elastoplastic finite element model was used to establish the relation between applied load and maximum tensile stress evolved on the lining surface. A 2D plane strain section approximated the sample geometry; interlayer and backing thickness are given in Table 1, while the lining thickness was assumed to be 0·25 mm. Point loads and constraints were

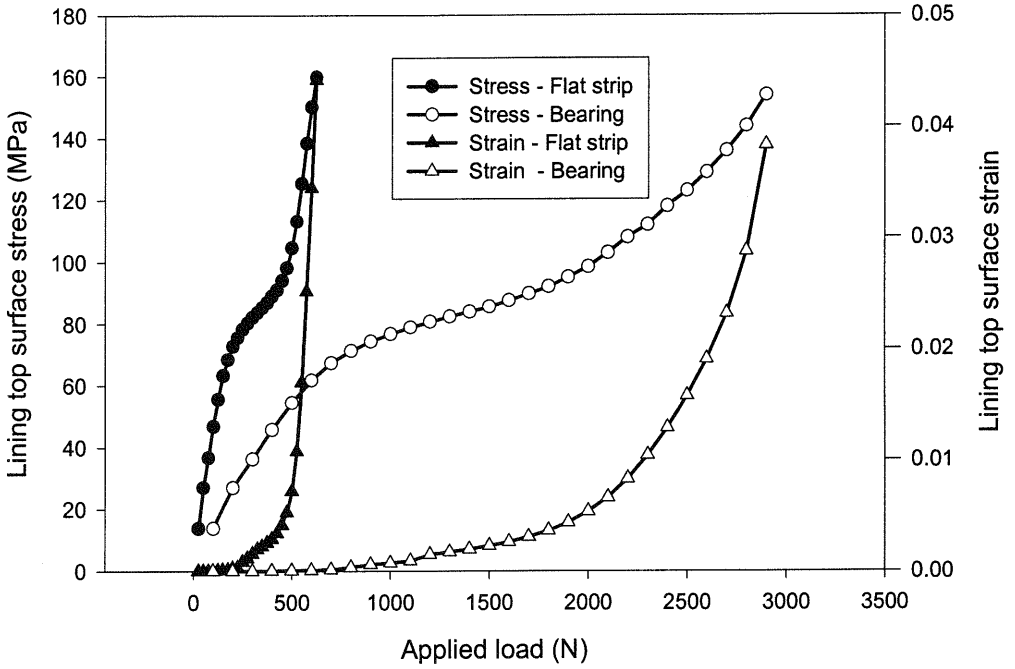

7 Predicted stress and strain at lining surface in bearing and flat strip samples

applied as appropriate for a three point loading geometry. The material model employed was identical to that used in the previous bearing model. The results obtained are plotted in Fig. 7.

Based on the behaviour of an initial test, a compliance failure criterion was defined in a similar manner to that used previously in the bearing tests. Failure was deemed to have occurred when the sample deflection at maximum load had increased from its initial value by 0·5 mm. A higher value is used to define the failure of flat strip tests compared to the bearings, since the flat strip test geometry is more compliant than the bearing rig. A deflection increase of 0·5 mm in a flat strip sample was found to correspond to a similar amount of fatigue cracking as that required to give a 0·3 mm deflection increase in a bearing sample.

All flat strip tests were carried out at a frequency of 10 Hz and with a load ratio of 0·1. The magnitude of this loading was such that the predicted maximum stress evolved on the surface of the lining at maximum load was 105 MPa. Vacuum tests were carried out using an ESH environmental chamber, which reliably produced vacuum levels of $1{\cdot}5 \times 10^{-5}$ mbar or lower. In the oil tests the sample was immersed in Shell Rotella X. This grade of oil (10W, kinematic viscosity 43·18 $mm^2\ s^{-1}$, density 876 kg m^{-3} at 40°C) is used by the sponsoring company in their bearing test programme.

Sample compliance was monitored throughout the test in all environments. However, detailed crack monitoring via surface replication was only carried out for tests in air and oil, since the time required for multiple vacuum pump down cycles was excessive. After testing, these replicas and the top surface of the failed samples were examined using optical microscopy (OM) and scanning electron microscopy (SEM). To allow investigation of the subsurface crack behaviour, samples were sectioned, polished and examined, again using OM and SEM.

Results

BEARING TESTS

Figure 8 shows the fatigue lifetimes obtained from the bearing tests as an $S-N$ curve. An endurance limit to 10^7 cycles was not obtained, the longest running test, at a stress range of 80 MPa gave a lifetime of 2×10^6 cycles. Since the bearing tests were carried out at stress levels

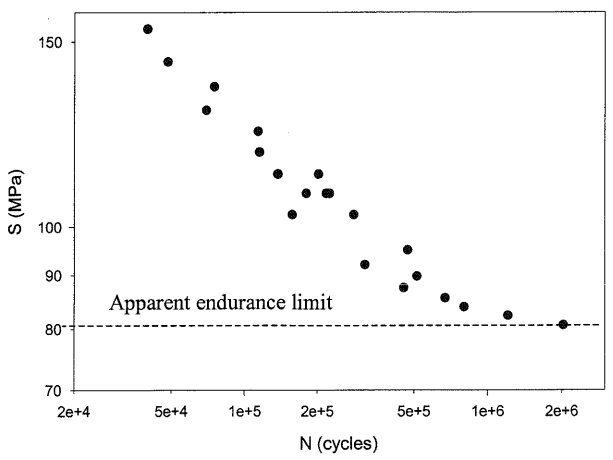

8 S–N curve of bearing fatigue test results

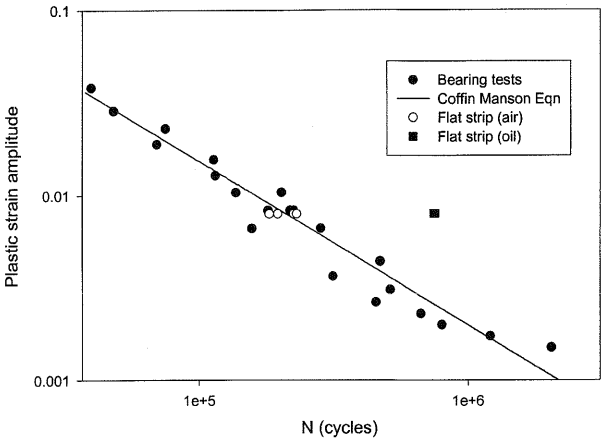

9 All fatigue test results plotted in terms of plastic strain amplitude

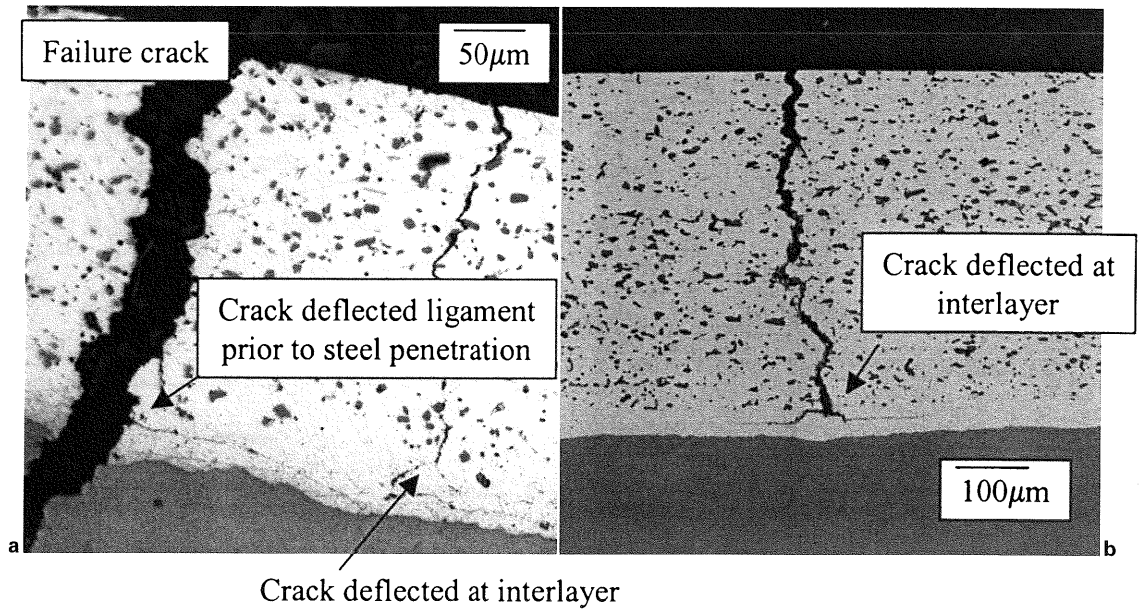

a bearing; *b* flat strip

10 Subsurface fatigue crack morphology in bearing and flat strip

considerably above the nominal monotonic yield stress (but below UTS), it was considered inappropriate to try to correlate the results with a stress life methodology. A strain–life approach was applied; Fig. 9 shows a graph of cycles to failure against plastic strain range. Equation (1), proposed by Coffin[4] and Manson[5] was then fitted to this data.

$$\frac{\Delta\varepsilon_p}{2} = \varepsilon_f'(2N_f)^e \quad \ldots\ldots\ldots\ldots\ldots\ldots \quad (1)$$

where ε_f' is the fatigue ductility coefficient and e is the fatigue ductility exponent. From the curve fit, these parameters were found to have values of 4·33 and −0·89 respectively. The strain–life model fits the data reasonably well since the strain–life methodology is able to account for the plastic deformation occurring within the lining material.

The failure criterion used resulted in visible fatigue cracks on the surface of the lining material, typically extending over 90–100% of the bearing width. The deflection at maximum load was seen to remain unchanged for ~95% of the specimen fatigue life, before increasing rapidly to the compliance failure condition. Figure 10*a* shows a section through a typical failed bearing. Fatigue cracks were observed to initiate at the lining free surface and propagate towards the steel backing. However, it appears that upon reaching the interlayer, the crack deflects or bifurcates and grows for a considerable distance normal to the interface. One of the cracks shown in Fig. 10*a* is still in this condition, while the other shows evidence of previous propagation in this manner, although it has now penetrated the steel layer, causing final sample failure.

Table 2 Fatigue lifetimes for all short crack tests

Sample	Environment	Test type	Lifetime, cycles
FSA1	Air	Uninterrupted	224347
FSA2	Air	Uninterrupted	195764
FSA3	Air	Replication	181986
FSA4	Air	Replication	229948
FSV1	Vacuum	Uninterrupted	1300000*
FSV2	Vacuum	Uninterrupted	2576629*
FSV3	Vacuum	Uninterrupted	5039397*
FSO1	Oil	Uninterrupted	754579
FSO1	Oil	Replication	747368

*Sample did not reach compliance failure.

FLAT STRIP TESTS

Fatigue lifetime

The fatigue lifetimes for the flat strip samples tested in all environments are shown in Table 2. Figure 9 shows the flat strip test lifetimes plotted on the strain–life curve established from the bearing tests. It is clear that the data from the air flat strip tests correlates well with the bearing lifetimes, the results falling well within the band of behaviour defined by the bearing tests. The lifetimes of the two oil tests were approximately 3·5 times that of the air tests, while no failures were achieved under vacuum conditions even after excessive numbers of cycles (more than $25N_{f\ air}$).

Fatigue initiation

Considering the replica record from both the air and oil tests, cracks were seen to initiate at multiple sites on the lining material surface, in the region of tensile lining stress. Fatigue crack initiations were first observed in air after 10 000 cycles and in oil after 40 000 cycles; at a similar fatigue life fraction of ~5% in both cases. Subsequent crack initiations continued throughout the duration of the test in both environments.

Initiation sites appeared to be associated with the Si phase rather than other secondary phases or slip bands as Shenton[1] reported. Figure 11 shows an SEM micrograph of a typical initiation site at higher magnification. It appears that fatigue cracks have initiated at the interface between the Si phase and the surrounding matrix; subsequent propagation has caused the Si phase to practically decohere. While no distinct fatigue initiation sites were evident in the sample tested in vacuum, evidence of voiding was seen on the sample surface as shown in Fig. 12.

Short crack growth behaviour

Short crack growth rates were collected from the replica records of the flat strip tests in both air and oil environments. Short crack ΔK levels were calculated using equation (2), suggested by Scott and Thorpe[6] for all short

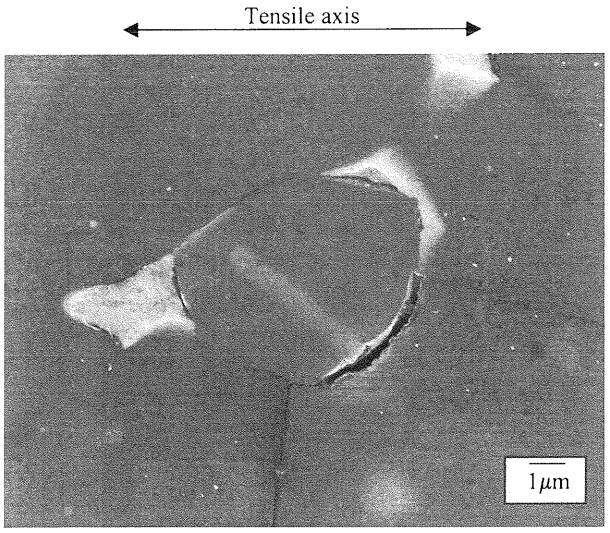

11 Typical fatigue crack initiation site associated with Si secondary phase

cracks measured.

$$K_s = \left[\left[M_{f(0)}\left(1-0{\cdot}3\,\frac{a}{W}\right)\left(1-\left(\frac{a}{W}\right)^{12}\right)\right] + \left[0{\cdot}394E(k)\left(\frac{a}{W}\right)^{12}\sqrt{\frac{c}{a}}\right]\right]\frac{\sigma_{max}}{E(k)}\sqrt{\pi a}$$

where

$$M_{f(0)} = \left[1{\cdot}21-0{\cdot}1\left(\frac{a}{c}\right)+0{\cdot}1\left(\frac{a}{c}\right)^4\right]\sqrt{\frac{a}{c}}$$

$$E(k) = \left[1+1{\cdot}47\left(\frac{a}{c}\right)^{1{\cdot}64}\right]^{1/2} \quad \ldots\ldots\ldots\ldots \quad (2)$$

The results are shown in Fig. 13. In both cases classic[7] short crack growth behaviour is seen, with characteristic crack growth rate increases and periods of arrest. It is also clearly shown that short crack fatigue growth is considerably higher in air than in oil.

Figures 14 and 15 show the lining surface at a life fraction of ~50% in air and oil respectively. Numerous short cracks are evident, propagating in a typically microstructurally sensitive manner. Occasional periods of linear growth occur in the matrix, apparently along slip bands. Secondary phases are evident along the crack path, the crack propagating through the Sn phase and along the Si/matrix interface

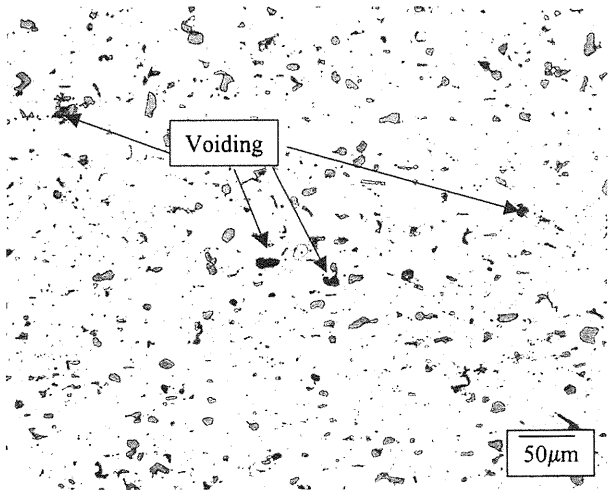

12 Surface voiding in vacuum test, possibly caused by decohered Si

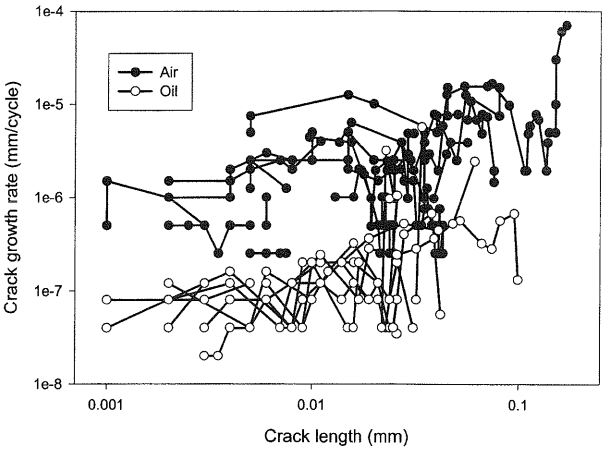

13 Comparison of short crack fatigue growth rates in air and oil

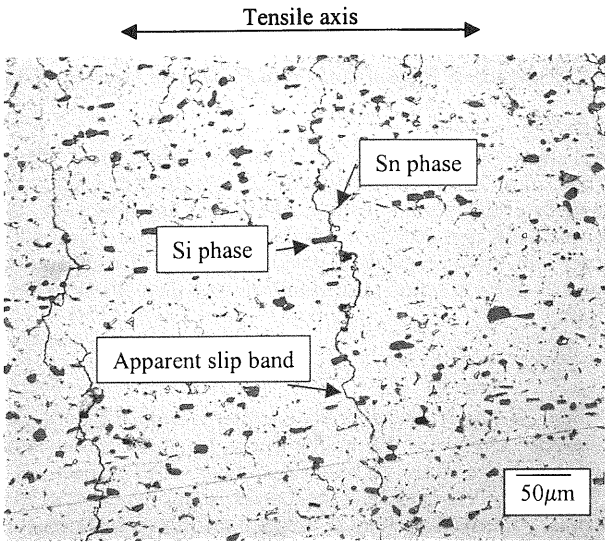

14 Optical micrograph of fatigue crack propagation in air showing microstructural interaction (N/N_f=50%)

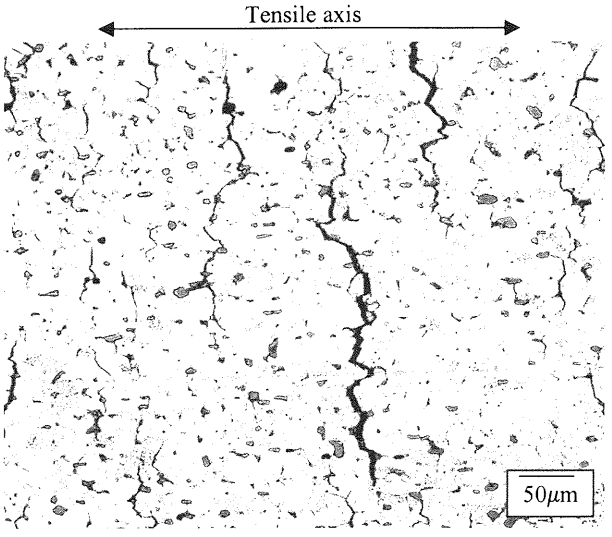

15 Optical micrograph of fatigue crack propagation in oil showing microstructural interaction (N/N_f=50%)

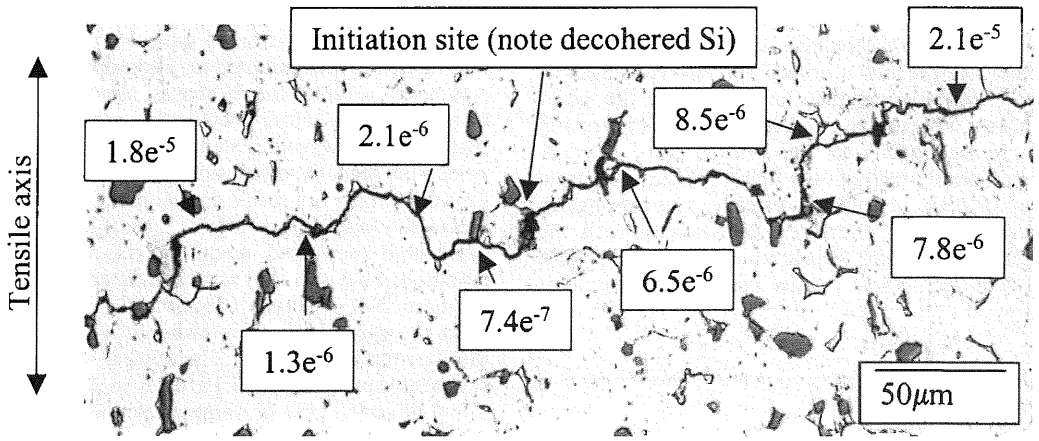

16 Annotated optical micrograph showing effect of microstructure on growth rate (mm cycle^{-1}) of typical short crack in air

respectively. In addition to obvious deviations in fatigue crack paths, considerable fluctuations in the growth rate were also observed. With reference to the replica record it was possible to relate these to microstructural interactions at the crack tip. This analysis was restricted to 40 cracks, and an example is shown in Fig. 16, annotated with the instantaneous growth rates at several points along its length. It appears that the impinging Si phases tend to retard crack growth, compared to propagation through either Sn phases or matrix. In contrast propagation rate along apparent matrix slip bands appears accelerated.

Short crack coalescence

Due to the density of initiation sites in both air and oil, clusters of microcracks coalesced rapidly to form larger cracks. Coalescence was first observed at lifetime fractions of ~25%, and continued to occur throughout the test as a dominant crack formed through successive events. Figure 17*a*–*e* show schematically how the crack field on the surface of sample FSA2 developed (the total number of cracks has been considerably reduced for clarity). Cracks first appeared towards one side of the sample; those in the region of maximum bending stress coalesced to form a dominant crack, and this crack then extended across the sample surface. A field of new cracks were seen to initiate rapidly ahead of the dominant crack; these grew rapidly and coalesced with the main crack, extending its length. Typically the main crack had extended over at least 90% of the sample width before a compliance failure condition was reached.

It was observed that as the projected distance between two coalescing cracks decreased, their growth rate accelerates markedly. Many cracks were seen to approach obliquely, a typical example is shown in Fig. 18. The cracks accelerated and grew in a direction normal to the direction of nominal stress, as the projected spacing between them decreased. However, once an overlap was established (projected spacing <0) their crack growth rate dropped markedly and they deflected towards each other, indicating a marked change in crack tip conditions.

As is shown in Fig. 17*c*–*e*, cracks propagating off the axis of maximum stress were often overtaken by the dominant crack. When this occurred their growth rate was seen to reduce considerably, usually arresting entirely.

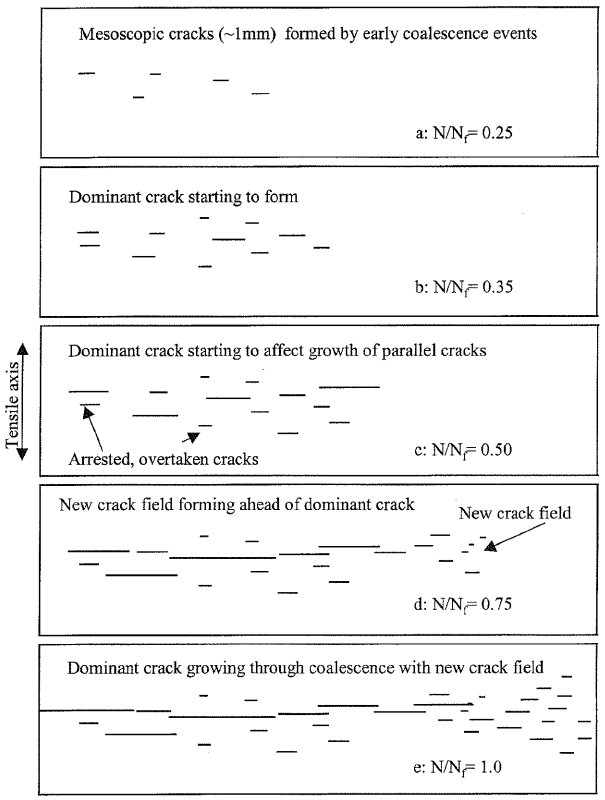

17 Schematics showing development of crack field on sample surface in ambient conditions

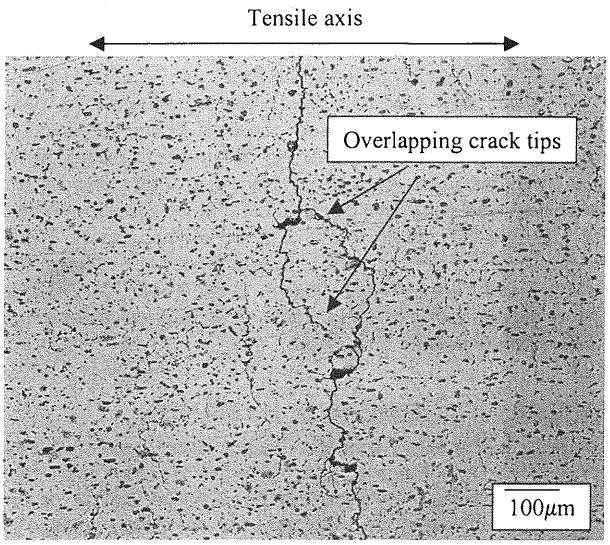

18 Typical crack coalescence behaviour of obliquely impinging cracks

Crack morphology at failure

The growth rate of large uncoalesced cracks was also seen to decrease once they reached a critical top surface length of 0·7–1·0 mm. Sectioning studies linked this to the point when the lining material is cracked through. Figure 10*b* shows that, in common with the bearing tests, a crack having grown entirely through the lining will not penetrate into the steel. Rather, it deflects abruptly, and propagates along the centre of the interlayer. In common with the bearing tests, final failure appeared to be caused by a previously deflected crack finally penetrating the steel backing.

Discussion

METHODOLOGY

The typical morphology of fatigue failure seen in an industrial accelerated bearing test rig is by lining failure. Cracks formed at the bearing surface propagate downwards to the steel backing, at which point they deflect and grow along the interface. Several such cracks eventually coalesce and cause a section of bearing lining to become detached (spall). This in turn leads to a gross reduction in bearing performance and hence the increase in oil temperature indicative of failure in Sapphire type machines. Similar behaviour, including highly deflected subsurface growth has also been observed under the highly simplified stress state employed in this study. Only the final failure mode is clearly different, spalling was not apparent since the stresses are concentrated rather than distributed over the bearing surface. Instead, final failure occurs when a previously deflected crack enters the backing layer. The use of a compliance failure condition was found to be successful in terminating the test shortly after this occurred.

It is believed that while the final failure mode clearly differs, the ability to closely monitor the initiation and early short crack growth afforded by the simple specimen design provides a valuable mechanistic insight into the parameters controlling the fundamental fatigue behaviour of these materials.

FATIGUE LIFETIME

An $S-N$ curve was produced using multiple uninterrupted tests on finished bearings. Although an endurance limit to 10^7 cycles was not established, the stress range necessary to cause failure in 2×10^6 cycles was such that its maximum stress was 142% of yield (46% UTS). Given that in this region the S–N curve is clearly approaching a limit, it is unlikely that the true endurance limit will be much lower.

A strain–life approach was able to collapse the data more effectively, as might be expected given the level of plastic strain evolved in the lining. When the lifetimes of the flat strip tests are plotted, it was seen that tests in air correlate well with the bearing behaviour. In comparison the fatigue lifetimes for the test in oil are considerably higher, while samples tested at identical loads in vacuum did not fail even after several million cycles ($\times25$ the lifetime observed in air). This indicates a strong environmental influence on fatigue behaviour.

SHORT FATIGUE CRACK INITIATION

In both air and oil, multiple fatigue cracks were seen to initiate early in the specimen's life ($N/N_f<5\%$), although subsequent initiations occurred throughout the life of the specimen. Initiation sites occurred on the lining surface in the region of maximum stress, at the interfaces between Si secondary phases and the surrounding matrix. Shenton *et al.*[1] also reported initiation from slip bands in this alloy, but initiations of this type were not observed in the current work. Close examination of typical initiation sites showed that fatigue cracks initiated at, and apparently grew almost completely around, the Si phases, almost decohering them from the matrix before propagating away. While no fatigue cracks were observed in samples tested in vacuum, surface voids were seen, the dimensions of which are consistent with the voids being the result of decohered Si particles.

Kumai *et al.*[8,9] observed this type of initiation in Al–SiC particulate reinforced metal matrix composite (PMMC) materials. They saw that cracks initiated from cracked large SiC particles (~300 μm^2) or in the absence of such features, from the debonding of smaller particles (~20 μm^2) from the surrounding matrix. The typical size distribution (1 standard deviation) of Si particles in the bearing lining is 1·7–13·8 μm^2. This is comparable with the smaller SiC particles, and hence the observed debonding in our materials is consistent with their findings.

EARLY SHORT FATIGUE CRACK PROPAGATION BEHAVIOUR

In both air and oil tests, early fatigue crack growth rate was seen to be highly microstructurally sensitive. Changes in crack growth rate may be seen clearly in the da/dN versus ΔK behaviour; such scatter in crack growth rates is typical of short crack fatigue behaviour.[10] In comparison to air, fatigue crack growth rate was reduced in oil and apparently suppressed in vacuum. The microstructural interaction was similar in air and oil, the fatigue path was reasonably tortuous and appeared to be preferentially seeking out secondary phases. Cracks propagated through the soft Sn phase, but around the harder Si phase, along the particle/matrix interface. This second event was linked to a reduction in crack growth rate. Similar behaviour has been reported in Al–Si cast alloys[11,12] and Al–SiC composites[13,14] in which small fatigue cracks are seen to deflect towards, and grow along the interfaces of the SiC inclusions. A reduction in crack growth rate at particle impingement was also reported by Kumai *et al.*,[8] who showed that cracks propagated at reduced rates along the interface of SiC particles in Al–SiC PMMC materials.

SHORT CRACK COALESCENCE BEHAVIOUR

In both air and oil tests the dominant failure crack was built up by successive coalescences. Due to the multiplicity of fatigue initiations these events were frequent and consequently the growth of a dominant crack was rapid. Several workers have observed this type of behaviour. The formation of such a crack was characterised in terms of a 'dominant effective short fatigue crack' by Zhao *et al.*[15] and as a 'major crack' by Gao *et al.*[16] Furthermore it was seen that, as cracks neared coalescence (based on projected spacing), their growth rate increased markedly. In addition to experimental observations made by several workers, this behaviour has been the subject of finite element analysis. Soboyejo *et al.*[17,18] showed that during the coalescence of a pair of colinear semielliptical cracks, the stress intensity factors (and hence growth rate) along their approaching fronts increased markedly, before dropping off as the crack evolved to a smooth elliptical profile.

Cracks propagating parallel to, but remote from, the area of maximum lining stress were seen to decelerate or arrest entirely when overtaken by the dominant crack. This is indicative of a stress shielding mechanism, which has been the subject of both experimental and finite element investigation by several authors. Soboyejo *et al.*[19] showed that given two or more parallel cracks, the larger will retard the growth of the smaller crack(s) until they become non-propagating. Obviously the event of a dominant crack overtaking a microcrack is a more extreme case; therefore the

retardation in microcrack growth rate is seen as almost immediate arrest.

Meyer *et al.*[20] investigated the general behaviour of interacting cracks. Employing finite element modelling and neural network approaches, criteria based on the *J*-integral were formulated for coalescence based on crack orientation. Their predictions for the behaviour of parallel and colinear cracks of unequal length agrees well with the behaviour observed in the bearing lining material. Parallel but non colinear cracks were seen to accelerate and continue growing normal to the applied stress field until they overlapped. Subsequent to this, their growth rate decreased markedly and their tips deflected towards each other, indicating a marked change in the crack tip driving force.[19,21] It is believed that this is due to mode mixity caused by the interaction of the stress strain fields surrounding the approaching crack tips. Again the experimental observations made in the current work agree with those of other workers and with analytical studies.

SUBSURFACE FATIGUE CRACK BEHAVIOUR

Uncoalesced cracks were observed to either considerably reduce in growth rate or arrest entirely when they reached a surface length of 0·7–1·0 mm, sectioning studies were used to assess this behaviour in terms of the subsurface behaviour. It was seen that a crack having propagated downwards through the lining material would deflect along the interlayer for some distance rather than immediately growing into the steel backing. Final failure was ultimately caused by a previously deflected crack penetrating the steel layer, causing a drastic increase in compliance. However, prior to this point the bearing's multilayer structure appears to exert a strong influence on the crack morphology.

Other workers have reported crack growth retardation and deflection associated with a bimaterial interface. Suresh *et al.*[22] considered the fatigue behaviour of a bimaterial comprising ferritic and austenitic steels, these materials having similar elastic properties and yield stress, but differing strain hardening rates, ultimate tensile stress and hence hardness (c.f. austenitic HV $\approx$200, ferritic HV $\approx$125). They observed that a fatigue crack approaching normal to the interface from the harder side, would pass through the interface undeflected, but a crack approaching from the softer side showed reduced crack growth rate, crack deflection, and finally arrest. This demonstrated that an interface between plastically dissimilar materials had the potential to severely affect the propagation behaviour of an impinging fatigue crack. Suresh *et al.* proposed two mechanisms to explain this behaviour. On a continuum mechanics basis, it was proposed that the local compliance ahead of the crack is reduced in the case of a crack approaching the interface from the softer side, and raised when the crack approaches from the harder side. It was argued that such a reduction in local compliance precludes continued crack propagation in the nominal mode I direction, hence the crack deflects. Using a micromechanics approach, it is argued that when a crack approaches an interface from the softer side, cyclic slip into the harder material becomes more difficult and the crack deflects as it seeks material with a lower resistance to fracture, the crack deflection then causing a marked reduction in crack tip driving force, and hence arrest.

The layered structure of the bearings considered in this paper is more complex than that of the simple steel bilayer considered by Suresh *et al.*, comprising as it does of three materials layers of both dissimilar elastic and plastic properties. Other workers[23–25] using analytical and finite element modelling techniques to characterise the influence of more complex interfaces on fatigue crack propagation behaviour have extended the work of Suresh *et al.* The implications of their findings on this bearing material system are discussed in greater detail in another paper by the authors.[26]

EFFECT OF ENVIRONMENT ON SHORT FATIGUE CRACK GROWTH

Vacuum conditions were expected to alter the fatigue behaviour, since it is known that fatigue mechanisms in aluminium alloys are highly sensitive to environmental changes. Several authors have found that fatigue crack growth rates may be as much as an order of magnitude lower under vacuum conditions than in moist air. This has been linked to the reduction in striation formation observed in samples tested in *vacuo*. Pelloux[27,28] hypothesised that the slip process by which striations form may be more reversible in the absence of an oxide layer, hence causing lower damage accumulation and therefore lower crack growth rates. In addition hydrogen embrittlement effects should be negligible under vacuum conditions, again promoting reduced crack growth rates.

Tests performed in an oil environment also typically showed a 3·5 times increase in lifetime compared with tests in air. The fatigue crack morphology in oil appears unchanged; only the growth rate is considerably reduced. Typically a small crack of given length will propagate at rates approximately an order of magnitude slower in oil than an equivalent crack in air conditions. This can be attributed to a number of factors affecting the conditions at the crack tip. Since the oil was not dehumidified, it is unlikely that it will provide an entirely inert environment at the crack tip,[29] and hence some degree of crack tip oxidation and hydrogen embrittlement may occur. Therefore it is not unexpected that crack growth in oil is more rapid than under vacuum. Tzou *et al.*[29] found that oils of viscosity less than 12 500 $mm^2\ s^{-1}$ reduced fatigue crack growth rates in steels and that this effect was greater in low viscosity oils. This was attributed to the low viscosity oil penetrating into the fatigue crack and causing the crack flanks to become prematurely closed on unloading.

The viscosity of the oil used in the flat strip tests was low (43·18 $mm^2\ s^{-1}$), also being paraffin based, it has a high surface tension, and thus it will easily penetrate into any fatigue cracks. Thus considering the tests were carried out at low load ratios, where closure mechanisms are known to have the greatest effect on fatigue crack growth rate,[30] and that the oil has almost certainly penetrated into the cracks, it is therefore likely that the crack will become wedged open during unloading. However, qualitative closure measurements could not be made during the test to confirm this.

The reduced crack growth rates in oil compared to air are therefore likely to be caused by a combination of fluid induced crack closure, and reduction of both hydrogen embrittlement and irreversible slip at the crack tip. However, the relative magnitudes of these effects cannot be established without further testing, which is beyond the scope of the present work.

Conclusions

1. Comparable failure morphology to that obtained in an industrial accelerated bearing fatigue rig may be produced using a three-point bend loading geometry. The ability to replicate the highly deflected subsurface growth indicates that the growth mechanism is essential unchanged. Therefore the detailed characterisation of fatigue made possible using the simplified loading geometry is applicable to more complex cases.

2. Multiple fatigue crack initiations were observed at the specimen surface; these were associated with the Si/matrix interface.

3. Early short fatigue crack growth was seen to be highly microstructural, and secondary phases appear to be preferentially sought out; the crack propagated around Si phases along their interfaces and through Sn phases. Crack

growth rate was retarded when Si particles impinged on the crack tip.

4. The dominant failure crack was built up through successive coalescence of microcracks.

5. An oil environment was found to increase the sample lifetime to ~3·5 times that of a comparable test in air. The crack growth mechanism appeared unchanged but the growth rate of individual cracks was severely retarded.

6. Vacuum was found to suppress crack growth, potential initiation sites were observed, but no fatigue crack growth was observed even after an excessive numbers of cycles.

This series of tests has provided insight into the fundamental fatigue behaviour of the bearing lining material. This information will be valuable for developing future candidate alloys for automotive bearing applications.

Acknowledgements

The authors would like to thank Dana Glacier Vandervell and the Engineering and Physical Sciences Research Council for financial and material support throughout the duration of this project.

References

1. P. SHENTON and C. PERRIN: Private communication, Dana Glacier Vandervell.
2. N. GYDE: 'Fatigue fracture in babbit lined journal bearings', PhD thesis, Technical University of Denmark, Copenhagen, 1969.
3. G. C. PRATT: *Int. Met. Rev.*, 1973, **18**, 62.
4. L. F. COFFIN: *Trans. ASME*, 1954, **76**, 15.
5. S. S. MANSON: 'National advisory commission on aeronautics: report 1170', 1954.
6. P. M. SCOTT and T.W. THORPE: *Fatigue Fract. Eng. Mater. Struct.*, 1981, **4**, 291.
7. S. SURESH and R. O. RITCHIE: *Int. Met. Rev.*, 1984, **29**, 445.
8. S. KUMAI, J. E. KING and J. F. KNOTT: *Fatigue Fract. Eng. Mater. Struct.*, 1992, **15**, 1.
9. S. KUMAI, J. E. KING and J. F. KNOTT: *Fatigue Fract. Eng. Mater. Struct.*, 1990, **13**, 511.
10. J. LANKFORD: *Fatigue Fract. Eng. Mater. Struct.*, 1982, **5**, 233.
11. K. SHIOZAWA, Y. TOHDA and S.-M. SUN: *Fatigue Fract. Eng. Mater. Struct.*, 1997, **20**, 237.
12. K. GALL, N. YANG, M. HORSTEMEYER, D. MCDOWELL and J. FAN: *Metall. Trans. A*, 1999, **30A**, 3079.
13. J. C. HEALY and C. J. BEEVERS: *Mater. Sci. Eng. A*, 1991, **A142**, 182.
14. M. JONO: Proc. 'Small fatigue cracks: mechanics, mechanisms and applications', Oahu, HI, USA, December 1998, The Engineering Foundation, 289.
15. Y. X. ZHAO, Q. GAO and J. N. WANG: *Fatigue Fract. Eng. Mater. Struct.*, 1999, **22**, 459.
16. N. GAO, M. W. BROWN and K. J. MILLER: *Fatigue Fract. Eng. Mater. Struct.*, 1995, **18**, 1423.
17. W. O. SOBOYEJO, K. KISHIMOTO, R. A. SMITH and J. F. KNOTT: *Fatigue Fract. Eng. Mater. Struct.*, 1989, **12**, 167.
18. W. O. SOBOYEJO and J. F. KNOTT: *Eng. Fract. Mech.*, 1990, **37**, 323.
19. W. O. SOBOYEJO and J. F. KNOTT: *Fatigue Fract. Eng. Mater. Struct.*, 1991, **14**, 37.
20. S. MEYER, E. DIEGELE, A. BRUCKNER-FOIT and A. MOSLANG: *Fatigue Fract. Eng. Mater. Struct.*, 2000, **23**, 315.
21. P. J. E. FORSYTH: *Acta Metall.*, 1983, **2**, 702.
22. S. SURESH, Y. SUGIMURA and E. K. TSCHEGG: *Scr. Metall. Mater.*, 1992, **27**, 1189.
23. Y. SUGIMURA, P. G. LIM, C. F. SHIH and S. SURESH: *Acta. Metall.*, 1995, **43**, 1157.
24. A. S. KIM and S. SURESH: *Int. J. Solids Structs.*, 1997, **34**, 3415.
25. R. PIPPAN, K. FLECHSIG and F. O. RIEMELMOSER: *Mater. Sci. Eng. A*, 2000, **A283**, 225.
26. M. R. JOYCE, P. A. S. REED and S. SYNGELLAKIS: *Mater. Sci. Eng. A*, 2003, **A342**, 11.
27. R. M. N. PELLOUX: *Trans ASME*, 1969, **62**, 281.
28. R. M. N. PELLOUX: *Eng. Fract. Mech.*, 1970, **1**, 697.
29. J. L. TZOU, S. SURESH and R. O. RITCHIE: *Acta. Metall.*, 1985, **33**, 105.
30. W. ELBER: 'Damage tolerant aircraft structure', STP 486, 230; 1971, Philadelphia, PA, ASTM.